Steel and Composite Structures, *Vol. 25, No. 5 (2017) 625-638*
DOI: https://doi.org/10.12989/scs.2017.25.5.625

Partial interaction analysis of multi-component members within the GBT

Alberto Ferrarotti[1,2], Gianluca Ranzi[*1], Gerard Taig[3] and Giuseppe Piccardo[2]

[1]*School of Civil Engineering, The University of Sydney, Sydney NSW 2006, Australia*
[2]*DICCA, Università degli Studi di Genova, Via Montallegro 1 – 16145 Genova, Italy*
[3]*ARUP, Sydney NSW 2000, Australia*

(*Received January 06, 2017, Revised August 25, 2017, Accepted September 03, 2017*)

Abstract. This paper presents a novel approach that describes the first-order (linear elastic) partial interaction analysis of members formed by multi-components based on the Generalised Beam Theory (GBT). The novelty relies on its ability to accurately model the partial interaction between the different components forming the cross-section in both longitudinal and transverse directions as well as to consider the cross-sectional deformability. The GBT deformations modes, that consist of the conventional, extensional and shear modes, are determined from the dynamic analyses of the cross-section represented by a planar frame. The partial interaction is specified at each connection interface between two adjacent elements by means of a shear deformable spring distributed along the length of the member. The ease of use of the model is outlined by an application performed on a multi-component member subjected to an eccentric load. The values calculated with an ABAQUS finite element model are used to validate the proposed method. The results of the numerical applications outline the influence of specifying different rigidities for the interface shear connection and in using different order of polynomials for the shape functions specified in the finite element cross-section analysis.

Keywords: generalised beam theory; partial interaction; steel-concrete members; thin-walled members

1. Introduction

Multi-component members are made by combining and interconnecting different structural elements to achieve a greater structural performance than the one exhibited by the combined contribution of the structural elements considered in isolation, e.g. built-up cold-formed members or members combining cold-formed thin-walled sections with concrete components. The multi-component response is highly dependent on the interface connection properties specified between adjacent components (i.e., partial shear interaction). The first model describing the partial interaction behaviour was proposed by Newmark *et al.* (1951) for a two-layered composite steel-concrete beam. Since then, the model has been extended in the field of composite construction accounting for material and geometric non-linearities (e.g., Nguyen *et al.* 2014, Su *et al.* 2015, Li *et al.* 2016, Liu *et al.* 2016), concrete time effects (e.g., Al-Deen *et al.* 2015), shear-lag of the slab (e.g. Dezi *et al.* 2003, 2006), shear deformability of the steel and concrete components (e.g., Chackrabarti *et al.* 2012, Gara *et al.* 2014, Nguyen *et al.* 2014) and transverse partial interaction (e.g., Adekola 1968). When dealing with thin-walled members, different approaches have been proposed to predict their response, such as the Finite Strip Method (FSM) (e.g., Á dány and Shafer 2006, Eccher *et al.* 2008, Vrcelj and Bradford 2008), perturbation approaches (e.g., Luongo 2001) and the Generalised Beam Theory (GBT). The latter was first introduced by Schardt (e.g., Schardt 1989), while a significant contribution to this method of analysis was provided by Camotim and co-workers (e.g., Silvestre and Camotim 2002, Gonçalves *et al.* 2010). Its use was also applied to obtain reduced models in the buckling analysis performed within the FSM and finite element (FE) approaches (e.g., Á dány and Shafer 2008, Casafront and Marimon 2009). With the GBT model, the displacement field is assumed to be described by a linear combination of pre-determined (known) cross-section deformation fields (referred to as "modes"), depending on the only cross-section curvilinear abscissa, and unknown intensity functions (referred to as "amplitudes"), which are only relied to beam abscissa. In this way, the three-dimensional continuum problem is reduced to a simpler one-dimensional vector-valued one, where the amplitude functions are the only problem unknowns. The GBT approach requires two steps. In the first step a cross-section analysis is performed and is used to identify a set of deformation modes. The second step determines the member behaviour (member analysis) by solving a reduced equivalent 1-D problem and determining the intensity functions.

A composite beam considering thin-walled members coupled with concrete slabs within the framework of the GBT was presented by Camotim and co-workers (Silva *et al.* 2006, Gonçalves and Camotim 2010). In this work, the partial interaction behaviour was introduced in the longitudinal direction of the member by introducing appropriate deformation modes to account for the

*Corresponding author, Professor,
E-mail: gianluca.ranzi@sydney.edu.au

ISSN: 1229-9367 (Print), 1598-6233 (Online)

longitudinal slip. This model was further extended to account for the material nonlinearity and buckling in (Henriques *et al.* 2015) and (Henriques *et al.* 2016), respectively. A different approach was recently proposed in references (Taig and Ranzi 2015, Taig *et al.* 2015a) to include the longitudinal partial interaction for two-layered composite members and extended in reference (Taig and Ranzi 2016) to account, for the first time within the GBT procedure, for both transverse and longitudinal partial interaction.

In this context, this paper presents a new partial interaction model for the first-order (linear elastic) analysis of multi-component members formed by thin-walled and concrete sections developed using the dynamic GBT cross-section approach (e.g., Ranzi and Luongo 2011, Piccardo *et al.* 2014). The main contribution of this work is related to the development of the procedure for the GBT cross-section analysis used to determine the set of conventional, extensional and shear modes. These are used within the GBT framework to account for both transverse and longitudinal interaction of multi-component members. Uniformly distributed deformable elastic springs are used to describe the flexibility of the interface connections. The proposed approach is then validated using the numerical results determined with a refined finite element model developed in ABAQUS/Standard (Dassault Systèmes Simulia 2008) as reference.

2. GBT approach for multi-components

2.1 Basis of the approach

A multi-component thin-walled member, with length L, is assumed to be prismatic and formed by N components. In its undeformed configuration, the beam occupies the prismatic volume $V=A\times[0,L]$ generated by translating its cross-section A, with regular boundary ∂A, along a straight line perpendicular to the cross-section and parallel to the Z-axis of the orthonormal reference system $\{O;X,Y,Z\}$. Without any loss of generality, each component (depicted by an area A_i with $i=1,...,N$) is described by a set of thin flat plates. The proposed approach is applicable to cross-sections that are open, closed or partially-closed.

The displacement field of a generic point P lying on the plate mid-surface S can be described as

$$\boldsymbol{u}(s,z)=u(s,z)\boldsymbol{i}+v(s,z)\boldsymbol{j}+w(s,z)\boldsymbol{k} \tag{1}$$

where $u(s,z)$, $v(s,z)$ and $w(s,z)$ are the components of the displacement as shown in Fig. 1, $\boldsymbol{i}$, $\boldsymbol{j}$ and $\boldsymbol{k}$ are unit vectors, z and s are the member coordinate and the curvilinear abscissa. By making use of the GBT formulation, Eq. (1) can be rewritten as follows

$$\boldsymbol{u}(s,z)=\begin{bmatrix}\sum_{k=1}^{K}U_k(s)\varphi_k(z)\\ \sum_{k=1}^{K}V_k(s)\varphi_k(z)\\ \sum_{k=1}^{K}\Omega_k(s)\varphi_{k,z}(z)+\sum_{j=1}^{J}W_j(s)\psi_j(z)\end{bmatrix} \tag{2}$$

where subscript k specifies the deformation mode, $U_k(s)$ and $V_k(s)$ depict the displacement components in the tangential and transverse directions, $\Omega_k(s)$ describe the longitudinal displacements, $\varphi_k(z)$ represent the unknown amplitude function associated with the k-th mode, $W_j(s)$ is the j-th shear mode, whose unknown amplitude function is depicted as $\psi_j(z)$. Using Kirchhoff plate theory and considering the modes introduced in Eq. (2), the displacement field $\boldsymbol{d}(s,y,z)$ is written as follows

$$\boldsymbol{d}(s,y,z)=\begin{bmatrix}\sum_{k=1}^{K}\left(U_k-yV_{k,s}\right)\varphi_k\\ \sum_{k=1}^{K}V_k\varphi_k\\ \sum_{k=1}^{K}\left(\Omega_k-yV_k\right)\varphi_{k,z}+\sum_{j=1}^{J}W_j\psi_j\end{bmatrix} \tag{3}$$

The corresponding infinitesimal strain field $\boldsymbol{\varepsilon}=\left[\varepsilon_s^{(M)}\ \varepsilon_z^{(M)}\ \gamma_{sz}^{(M)}\ \varepsilon_s^{(F)}\ \varepsilon_z^{(F)}\ \gamma_{sz}^{(F)}\right]^T$ can be obtained from the kinematic strain-displacement relations. With the adopted notation M represents the membrane strains and F the flexural ones. The materials considered are isotropic and linear elastic. The constitutive representation for the α-th material ($\alpha=1,...,N_m$, being N_m the total number of material composing the multi-composed cross-section) can be expressed as

$$\boldsymbol{\sigma}_\alpha=\mathbf{E}_\alpha\boldsymbol{\varepsilon} \tag{4}$$

where $\boldsymbol{\sigma}_\alpha$ represents the stress field acting on the α-th material and $\mathbf{E}_\alpha$ represents its elastic matrix.

Eq. (4) can be re-written as follows in terms of the adopted displacement field

$$\boldsymbol{\sigma}_\alpha=\begin{bmatrix}\sigma_s^{(\alpha M)}\\ \sigma_z^{(\alpha M)}\\ \tau_{sz}^{(\alpha M)}\\ \sigma_s^{(\alpha F)}\\ \sigma_z^{(\alpha F)}\\ \tau_{sz}^{(\alpha F)}\end{bmatrix}=\begin{bmatrix}\frac{E_\alpha}{1-\nu_\alpha^2}\sum_{k=1}^{K}\left(U_{k,s}\varphi_k+\nu_\alpha\Omega_k\varphi_{k,zz}\right)+\frac{\nu_\alpha E_\alpha}{1-\nu_\alpha^2}\sum_{j=1}^{J}W_j\psi_{j,z}\\ \frac{E_\alpha}{1-\nu_\alpha^2}\sum_{k=1}^{K}\left(\nu_\alpha U_{k,s}\varphi_k+\Omega_k\varphi_{k,zz}\right)+\frac{E_\alpha}{1-\nu_\alpha^2}\sum_{j=1}^{J}W_j\psi_{j,z}\\ G_\alpha\sum_{k=1}^{K}\left(U_k+\Omega_{k,s}\right)\varphi_{k,z}+G_\alpha\sum_{j=1}^{J}W_{j,s}\psi_j\\ -y\frac{E_\alpha}{1-\nu_\alpha^2}\sum_{k=1}^{K}\left(V_{k,ss}\varphi_k+\nu_\alpha V_k\varphi_{k,zz}\right)\\ -y\frac{E_\alpha}{1-\nu_\alpha^2}\sum_{k=1}^{K}\left(\nu_\alpha V_{k,ss}\varphi_k+V_k\varphi_{k,zz}\right)\\ -2yG_\alpha\sum_{k=1}^{K}V_{k,s}\varphi_{k,z}\end{bmatrix} \tag{5}$$

in which E_α is the elastic modulus, G_α represents the shear modulus and ν_α is Poisson's ratio.

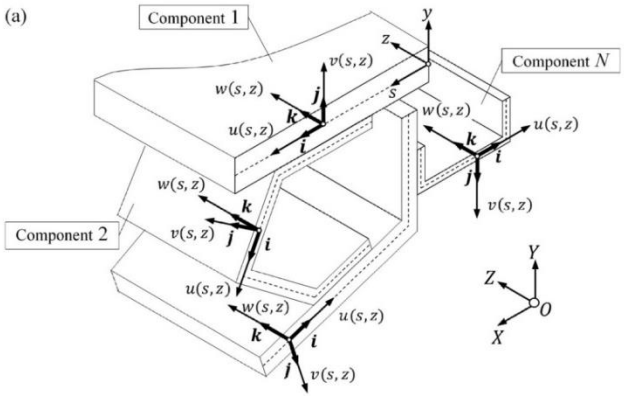

Fig. 1 Displacement field.

2.2 Partial interaction

The composite action is introduced using N_{SC} shear connections placed along rectilinear lines Λ_n (with n=1,..., N_{SC}) at the interface between the N components, similarly to what was recently proposed for composite two-layered thin-walled beams in references (Taig and Ranzi 2015, 2016, Taig *et al.* 2015a) (Fig. 2(a)). The shear connections are assumed to allow relative displacement between adjoining elements in both longitudinal (i.e., along the z coordinate) and transverse (i.e., along the s coordinate) directions, while separation of the adjacent elements is prevented. For the n-th shear connection, the domain of Λ_n that connects the i-th and j-th components of the cross-section is identified by the set of points $\left(s_n^{(i)}, y_n^{(i)}, z\right)$ and $\left(s_n^{(j)}, y_n^{(j)}, z\right)$ (Fig. 2(b)). The variables $s_n^{(i)}$ and $s_n^{(j)}$ define the location of the n-th shear connection along the mid-line C of the i-th and j-th components, while the variables $y_n^{(i)}$ and $y_n^{(j)}$ describe the perpendicular distance from the mid-surface S to the interface for the i-th and j-th elements, respectively (Fig. 2(b)). The longitudinal slip $\delta_L^{(n)}(z)$ and the transverse slip $\delta_T^{(n)}(z)$ can be determined for the n-th shear connection as (Fig. 2(c))

$$\boldsymbol{\delta}_n = \begin{bmatrix} \delta_T^{(n)}(z) \\ \delta_L^{(n)}(z) \end{bmatrix} = \begin{bmatrix} d_s(s_n^{(j)}, y_n^{(j)}, z) - d_s(s_n^{(i)}, y_n^{(i)}, z) \\ d_z(s_n^{(j)}, y_n^{(j)}, z) - d_z(s_n^{(i)}, y_n^{(i)}, z) \end{bmatrix} \quad (6)$$

where $d_s\left(s_n^{(k)}, y_n^{(k)}, z\right)$ and $d_z\left(s_n^{(k)}, y_n^{(k)}, z\right)$ depict the transverse and longitudinal slips calculated at the n-th connection interface extreme fibre of the generic k-th component. Eq. (6) can be expressed in the GBT context as a function of the deformation modes as follows

$$\boldsymbol{\delta}_n = \begin{bmatrix} \delta_T^{(n)}(z) \\ \delta_L^{(n)}(z) \end{bmatrix} = \begin{bmatrix} \sum_{k=1}^{K} \bar{V}_k^{(n)} \varphi_k \\ \sum_{k=1}^{K} \bar{\Omega}_k^{(n)} \varphi_{k,z} + \sum_{j=1}^{J} \bar{W}_j^{(n)} \psi_j \end{bmatrix} \quad (7)$$

where

$$\bar{V}_k^{(n)} = \left[U_k\left(s_n^{(j)}\right) - y_n^{(j)} V_{k,s}\left(s_n^{(j)}\right)\right] - \left[U_k\left(s_n^{(i)}\right) - y_n^{(i)} V_{k,s}\left(s_n^{(i)}\right)\right] \quad (8)$$

$$\bar{\Omega}_k^{(n)} = \left[\Omega_k\left(s_n^{(j)}\right) - y_n^{(j)} V_k\left(s_n^{(j)}\right)\right] - \left[\Omega_k\left(s_n^{(i)}\right) - y_n^{(i)} V_k\left(s_n^{(i)}\right)\right] \quad (9a)$$

$$\bar{W}_j^{(n)} = W_j\left(s_n^{(j)}\right) - W_j\left(s_n^{(i)}\right) \quad (9b)$$

The composite action is provided by the presence of uniformly distributed linear elastic springs where the behaviour of the n-th shear connection is expressed as

$$\boldsymbol{f}_n = \begin{bmatrix} f_T^{(n)}(z) \\ f_L^{(n)}(z) \end{bmatrix} = \begin{bmatrix} k_T^{(n)} \sum_{k=1}^{K} \bar{V}_k^{(n)} \varphi_k \\ k_L^{(n)} \left(\sum_{k=1}^{K} \bar{\Omega}_k^{(n)} \varphi_{k,z} + \sum_{j=1}^{J} \bar{W}_j^{(n)} \psi_j \right) \end{bmatrix} \quad (10)$$

in which vector $\boldsymbol{f}_n$ collects both the transverse and longitudinal forces per unit length induced in the spring, i.e., $f_T^{(n)}$ and $f_L^{(n)}$, while $k_T^{(n)}$ and $k_L^{(n)}$ are the transverse and longitudinal shear connection rigidities, respectively.

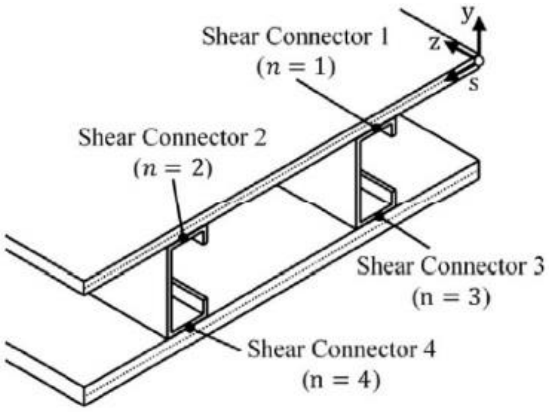

(a) Cross-section with shear connectors

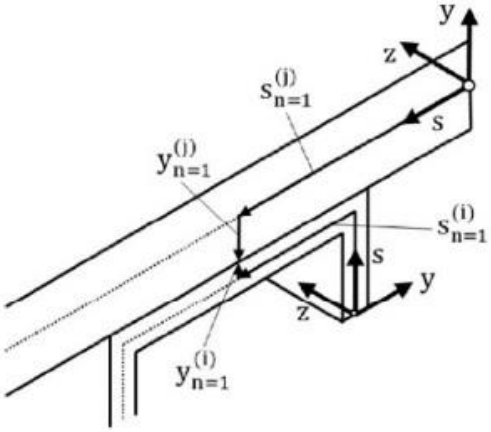

(b) Location of the shear connection

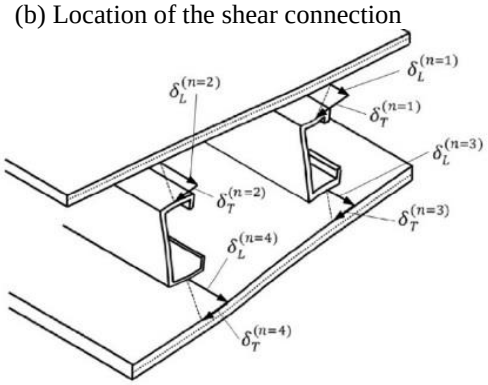

(c) Longitudinal and transverse slips

Fig. 2 Interface connection details

2.3 Member analysis

The weak form of the problem is derived by means of the principle of virtual work

$$\sum_{\alpha=1}^{N_m} \int_{V_\alpha} \hat{\boldsymbol{\varepsilon}}^T \boldsymbol{\sigma}\, dV + \sum_{n=1}^{N_{cs}} \int_L \hat{\boldsymbol{\delta}}_n^T \boldsymbol{f}_n\, dz = \sum_{\alpha=1}^{N_m} \int_{\partial V_\alpha} \hat{\boldsymbol{u}}^T \boldsymbol{p}\, dS \quad (11)$$

where the surface loads are collected in $\boldsymbol{p}(s,z) = p_s(s,z)\boldsymbol{i} + p_y(s,z)\boldsymbol{j} + p_z(s,z)\boldsymbol{k}$, the hat $\hat{}$ denotes a virtual quantity, V_α and ∂V_α describe the volume and the surface area of the α-*th* material. From the assumed displacement fields and constitutive models described above, the weak form can be expressed in compact form as follows

$$\int_L \left(\boldsymbol{A}\hat{\boldsymbol{d}}\right)^T \mathbf{B}\left(\boldsymbol{A}\boldsymbol{d}\right) dz = \int_L \left(\boldsymbol{B}\hat{\boldsymbol{d}}\right)^T \boldsymbol{q}\, dz \quad (12)$$

where **B** is the stiffness matrix, $\boldsymbol{d} = [\boldsymbol{\varphi}; \boldsymbol{\psi}]$, $\boldsymbol{q}$ is the loading vector, and $\boldsymbol{A}$ and $\boldsymbol{B}$ represent differential operators. All terms are defined in Appendix.

Eq. (12) is solved using the finite element method by approximating the generalised displacements $\boldsymbol{d}$ with polynomial shape functions, i.e., $\boldsymbol{d} \cong \boldsymbol{N}_d^e\, \boldsymbol{d}^e$ where the shape functions are specified in matrix $\boldsymbol{N}_d^e$ with dimensions of $(K+J)\times(4K+3J)$ and $\boldsymbol{d}^e$ is the generalised nodal displacements $(4K+3J)$ vector. Cubic (Hermitian) polynomial and parabolic (Lagrangian) polynomials are adopted as shape functions for $\boldsymbol{\varphi}$ and $\boldsymbol{\psi}$, respectively. The finite element representation can then be rewritten in compact form as follows

$$\mathbf{K}^e \boldsymbol{d}^e = \boldsymbol{p}^e \quad (13)$$

where the stiffness matrix $\mathbf{K}^e$ and the load vector $\boldsymbol{p}^e$ are defined as

$$\mathbf{K}^e = \int_L \left(\boldsymbol{A}\boldsymbol{N}_d^e\right)^T \mathbf{B}\left(\boldsymbol{A}\boldsymbol{N}_d^e\right) dz \quad (14)$$

$$\boldsymbol{p}^e = \int_L \left(\boldsymbol{B}\boldsymbol{N}_d^e\right)^T \boldsymbol{q} dz \quad (15)$$

The first-order (linear elastic) analysis is then carried out based on the finite element method, e.g., (Bathe 2006, Ranzi and Gilbert 2015).

3. Cross-section analysis

This section presents the procedure to evaluate the basis of GBT deformation modes (i.e., conventional, extensional and shear modes) suitable to describe the partial interaction behaviour of multi-component members. In particular, the conventional modes are derived from Vlasov's theory (Vlasov 1961) based on the conditions of membrane unshearability and (transverse) inextensibility. In the case of closed loops, the former condition is replaced by Bredt's hypothesis. As a consequence, conventional planar modes may be supplied with linear warping distributions with discontinuities at shear connection locations. Extensional modes are associated to non-nil in-plane elongation of the cross-section elements and nil warping. The shear modes are depicted by nil in-plane deformation and non-nil warping distributions.

The determination of the conventional, extensional and shear modes is carried out by solving two eigenproblems following the procedure of the (dynamic) GBT-D approach previously proposed by the authors for the identification of the conventional, extensional and shear modes, e.g. (Ranzi and Luongo 2011, Piccardo *et al.* 2014, Taig *et al.* 2015b). In particular, one eigenvalue problem is used for the identification of the planar deformations modes associated with the conventional and extensional modes. For ease of reference, this is referred to as planar eigenvalue problem (PEP) and is described in Section 3.1. A second eigenproblem is required for the characterization of the warping components associated with the shear modes, denoted as the warping eigenvalue problem (WEP). The WEP is outlined in Section 3.2. The warping components of the conventional modes are determined by post-processing the results of the PEP solution. No additional calculations are required for the extensional or shear modes because they do not possess warping or in-plane deformations, respectively, in their modes based on the representation adopted in this paper.

With this approach, the multi-component cross-section is represented by a frame unconstrained in its plane and discretized using the finite element method as shown, for illustrative purposes, in Fig. 3 reconsidering the cross-section of Fig. 1.

3.1 Planar eigenvalue problem (PEP)

The PEP relies on the use of a planar extensible frame for the representation of the cross-section (Fig. 3). The numerical calculation of the dynamic modes of the frame is performed by means of the finite element method, e.g. (Bathe 2006, Ranzi and Gilbert 2015). In the spirit of the GBT-D, the frame's dynamic modes correspond to the modes sought for the GBT basis.

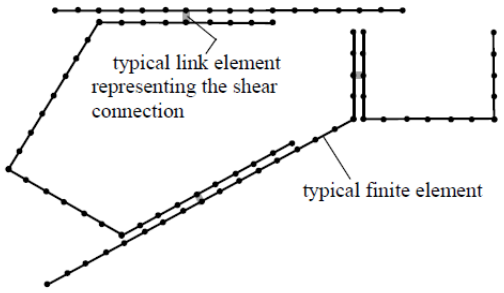

Fig. 3 Example of finite element discretization presented by considering the multi-component cross-sections illustrated in Fig. 1

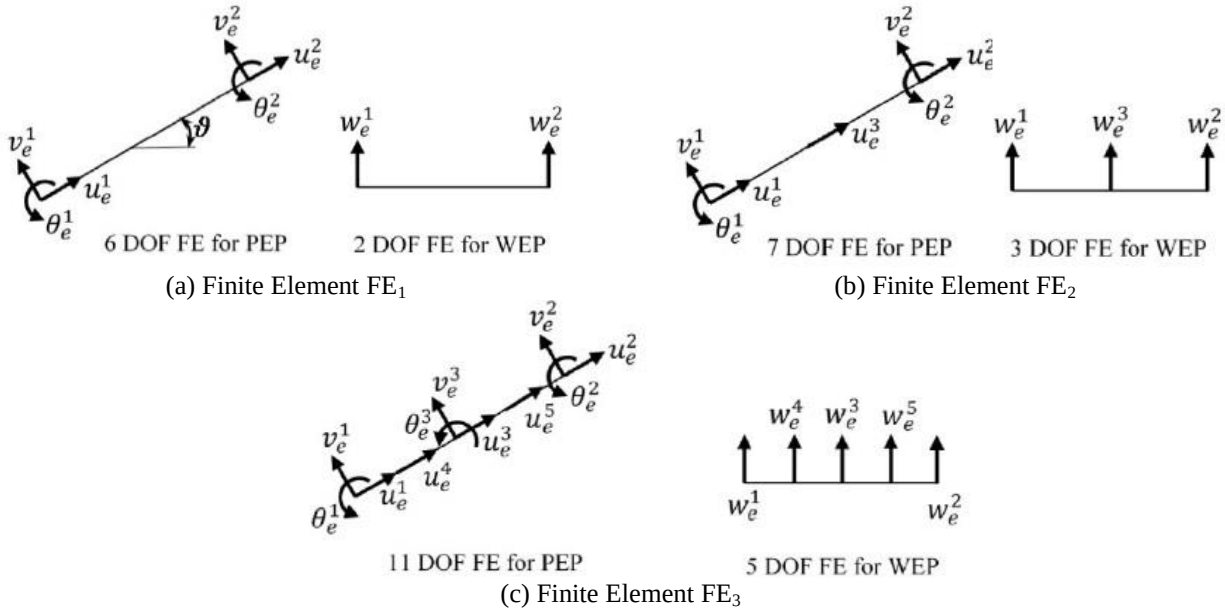

(a) Finite Element FE_1 (b) Finite Element FE_2

(c) Finite Element FE_3

Fig. 4 Nodal (local) degree of freedoms of finite elements used in the cross-section analysis

In the numerical implementation, the cross-section of the multi-component is discretised using one-dimensional finite elements. In this study, three finite elements are considered for the PEP to evaluate the possible implications of adopting different approximations for the model generalized displacements and how these influence the GBT numerical description. The three finite elements are referred to in the following as: (i) FE_1 (Fig. 4(a)) which depicts a 6 DOF finite element with linear (Lagrangian) and cubic (Hermitian) polynomial shape functions describing the axial and transverse displacement, respectively; (ii) FE_2 (Fig. 4(b)) that represents a 7 DOF finite element with parabolic (Lagrangian) and cubic (Hermitian) shape functions; and (iii) FE_3 (Fig. 4(c)) that depicts a 11 DOF finite element with quartic (Lagrangian) and quintic (Hermitian) polynomials approximating the axial and transverse displacement, respectively. Assembling the contribution of each element, the problem can be expressed as an algebraic eigenvalue problem

$$\left(\mathbf{K}_P - \lambda \mathbf{M}_P\right)\boldsymbol{q}_P = \mathbf{0} \tag{16}$$

where λ and $\boldsymbol{q}_P$ are the eigenpair, while $\mathbf{K}_P$ is the frame stiffness matrix and $\mathbf{M}_P$ represents its mass matrix.

Linear elastic springs with negligible mass are specified at the location of the shear connections to account for the flexibility present in the transverse direction between adjacent components. This is carried out using the spring finite element depicted in Fig. 4(a) whose stiffness matrix $\mathbf{K}_P^{(n)}$ is

$$\mathbf{K}_P^{(n)} = k_T^{(n)} \begin{bmatrix} 0 & 0 & 0 & 0 & 0 & 0 \\ & 1 & 0 & 0 & -1 & 0 \\ & & 0 & 0 & 0 & 0 \\ & & & 0 & 0 & 0 \\ & \text{sym} & & & 1 & 0 \\ & & & & & 0 \end{bmatrix} \tag{17}$$

Separation or penetration between adjacent components at their interface is prevented by enforcing an internal axial restraint to the 6 DOF link element representing the shear connection, therefore ensuring that the element remains inextensible along its length. In local coordinates, this can be written for the *n*-th link element (with end nodes *i* and *j*) by requiring its elongation to be zero (Fig 4(a))

$$u_n^{(j)} - u_n^{(i)} = 0 \tag{18}$$

A further internal constraint, to satisfy the in-plane rotation's compatibility, is applied to the rotations at the link element ends as follows (Fig. 4(a))

$$\theta_n^{(j)} - \theta_n^{(i)} = 0 \tag{19}$$

The $2N_{SC}$ constraint conditions specified in Eqs. (18) and (19) are re-written in global coordinates in the following form

$$\mathbf{A}\boldsymbol{q}_P = \begin{bmatrix} \mathbf{A}_M & \mathbf{A}_S \end{bmatrix} \begin{bmatrix} \boldsymbol{q}_{PM} \\ \boldsymbol{q}_{PS} \end{bmatrix} = \mathbf{0} \tag{20a}$$

where the N_{dof} nodal (global) displacements $\boldsymbol{q}_P$ are partitioned into $2N_{SC}$ slave displacements collected in $\boldsymbol{q}_{PS}$ and the K (= N_{dof} - $2N_{SC}$) master displacements $\boldsymbol{q}_{PM}$ as follows

$$\boldsymbol{q}_P = \begin{bmatrix} \boldsymbol{q}_{PM} \\ \boldsymbol{q}_{PS} \end{bmatrix} = \mathbf{R}\boldsymbol{q}_{PM}; \quad \mathbf{R} = \begin{bmatrix} \mathbf{I} \\ -\mathbf{A}_S^{-1}\mathbf{A}_M \end{bmatrix} \tag{20b,c}$$

The eigenvalue problem of Eq. (16) can then be rewritten considering the above internal constraints as

$$\left(\mathbf{K}_{PR} - \lambda \mathbf{M}_{PR}\right)\boldsymbol{q}_{PM} = \mathbf{0} \tag{21}$$

in which the reduced order ($K \times K$) stiffness $\mathbf{K}_{PR}$ and mass

$\mathbf{M}_{PR}$ matrices are defined as

$$\mathbf{K}_{PR} = \mathbf{R}^T \mathbf{K}_P \mathbf{R}; \qquad \mathbf{M}_{PR} = \mathbf{R}^T \mathbf{M}_P \mathbf{R} \tag{22a,b}$$

Eigenvectors $\boldsymbol{q}_P$ (obtained from $\boldsymbol{q}_{PM}$ using Eq. (20b)) contain the nodal displacements that define the in-plane deformation modes and that provide a mixed description of the conventional and extensional modes. Since the frame is unconstrained, the stiffness matrix $\mathbf{K}_P$ is positive semi-definite and Eq. (21) admits a triple nil eigenvalue representing rigid planar motions of the frame. They can be conveniently chosen as the two rigid translation along the principal inertia axis and a rotation with respect to the shear centre.

To obtain the set of modes commonly used in the GBT approach, the in-plane modes are now subdivided into those that are inextensible (i.e., conventional modes) and those that are free to extend (i.e., extensional modes). This procedure will produce N_C conventional modes and N_E (=K-N_C) extensional modes and is implemented by performing a change of base to the set of deformation modes after removing the three rigid modes, i.e., $\boldsymbol{Q}_P^*$=[$\boldsymbol{q}_{P4}$, $\boldsymbol{q}_{P5}$, ... $\boldsymbol{q}_{PK}$] by solving the following eigenproblem

$$\left(\mathbf{C} - \mu \mathbf{D}\right)\boldsymbol{u} = \mathbf{0} \tag{23}$$

where μ and $\boldsymbol{u}$ depict an eigenpair, matrices $\mathbf{C}$ and $\mathbf{D}$ have dimensions (K-3)×(K-3) and are defined in Appendix. In particular, $\mathbf{C}$ accounts for the axial deformations of the plate elements and $\mathbf{D}$ considers their flexural deformations.

Eq. (23) admits N_{CD} (=N_C-3) zero eigenvalues that represent the conventional (planar inextensible) modes (i.e. the conventional modes without the 3 in-plane rigid modes).

The remaining N_E (=K-N_C) non-zero eigenvalues depict the extensional modes. By collecting the eigenvectors $\boldsymbol{u}_i$ corresponding to the zero eigenvalues (i.e., i=1,…,N_{CD}) in the transformation matrix $\mathbf{T}_{CD}^* = \left[\boldsymbol{u}_1, \boldsymbol{u}_2, ..., \boldsymbol{u}_{N_{CD}}\right]$ and the remaining ones $\boldsymbol{u}_e$ corresponding to non-zero eigenvalues (i.e., i=N_{CD}+1,…,K-3) in the transformation matrix $\mathbf{T}_E^* = \left[\boldsymbol{u}_{N_{CD}+1}, ..., \boldsymbol{u}_i, ..., \boldsymbol{u}_{K-3}\right]$, the conventional and extensional modes can be separated through the following linear transformations

$$\begin{bmatrix} \mathbf{Q}_{CD}^{*\,T} \\ \mathbf{Q}_E^{*\,T} \end{bmatrix} = \begin{bmatrix} \mathbf{T}_{CD}^{*\,T} \\ \mathbf{T}_E^{*T} \end{bmatrix} \mathbf{Q}_P^{*\,T} \tag{24}$$

where $\mathbf{Q}_{CD}^*$ and $\mathbf{Q}_E^*$ are the modal matrices, whose columns represent the conventional (without the rigid modes) and extensional planar modes, respectively. Although this set of modes could already be used in the member analysis, a further post-processing is performed to ensure that all identified modes reflect the response of the entire cross-section, rather than just displacements of localised parts of it. This latter change of basis is performed by solving the following eigenproblem

$$\left(\mathbf{T}_{CD}^{*\,T} \mathbf{D} \mathbf{T}_{CD}^* - \mu_1 \mathbf{I}\right)\boldsymbol{v} = \mathbf{0} \tag{25}$$

from which the following transformation matrix $\mathbf{T}_{CD}$ is obtained

$$\mathbf{T}_{CD} = \left[\boldsymbol{v}_1, \boldsymbol{v}_2, ..., \boldsymbol{v}_{N_{CD}}\right] \tag{26}$$

Similarly, the basis of the extensional modes is revised by solving the eigenproblem

$$\left(\mathbf{T}_E^{*T} \mathbf{C} \mathbf{T}_E^* - \mu_2 \mathbf{I}\right)\boldsymbol{w} = \mathbf{0} \tag{27}$$

from which the transformation matrix $\mathbf{T}_E$ may be obtained

$$\mathbf{T}_E = \left[\boldsymbol{w}_1, \boldsymbol{w}_2, ..., \boldsymbol{w}_{N_E}\right] \tag{28}$$

The final sets of conventional (without the rigid modes) and extensional modes, in terms of nodal values, can be then evaluated based on the following linear transformations

$$\mathbf{Q}_{CD}^T = \mathbf{T}_{CD}^T \mathbf{Q}_{CD}^{*\,T}; \qquad \mathbf{Q}_E^T = \mathbf{T}_E^T \mathbf{Q}_E^{*\,T} \tag{29a,b}$$

The complete set of conventional (planar inextensible) modes is then composed by the three rigid-body modes (removed at the beginning of this procedure) and the modes provided by $\mathbf{Q}_{CD}$, i.e. $\mathbf{Q}_C$=[$\boldsymbol{q}_{P1}$,$\boldsymbol{q}_{P2}$,$\boldsymbol{q}_{P3}$,$\mathbf{Q}_{CD}$].

The procedure to evaluate the out-of-plane components associated with each conventional mode is described below based on Vlasov theory. This is carried out by enforcing (i) tangential inextensibility (already satisfied by the set $\mathbf{Q}_C$ previously derived), (ii-a) nil membrane shear strain and/or (ii-b) piecewise constant membrane shear strain, enforced by post-processing the in-plane deformation modes as usually carried out in the dynamic GBT approaches, e.g., (Taig and Ranzi 2016). With this approach and as a consequence of Vlasov theory, the unknown warping profiles are assumed to vary linearly within each element and their unknown distribution is conveniently described in terms of unknown nodal values. In particular, the warping at the i-th node of the cross-section considering the k-th deformation mode is denoted as $\Omega_k^{(i)}$. For each closed loop present in the cross-section, an additional unknown representing the tangential shear flow is introduced. The shear flow associated with the l-th loop is referred to as $Q_k^{(l)}$ for the k-th mode.

Conventional warping distributions are obtained by applying the following equation to each finite element used in the cross-sectional discretisation

$$G_\alpha t_e \left[\frac{1}{b_e}\left(\Omega_k^{(j)} - \Omega_k^{(i)}\right) + U_k^{(e)}\right] = \sum_l \pm Q_k^{(l)} \tag{30}$$

where the e-th finite element has length b_e, thickness t_e and shear modulus G_α, $\Omega_k^{(i)}$ and $\Omega_k^{(j)}$ describe the value at the first node i (i.e., at s=0) and the value at the second node j (i.e., at s=b_e), respectively, and $U_k^{(e)}$ depicts the element constant axial deformation. For plate elements part of open sections or branches, the shear flow is nil and right-hand side of Eq. (30) becomes zero, therefore simplifying to

$$\frac{1}{b_e}\left(\Omega_k^{(j)}-\Omega_k^{(i)}\right)+U_k^{(e)}=0 \tag{31}$$

For elements describing the shear connection components, the following condition is applied

$$k_L^{(n)}\bar{\Omega}_k^{(n)}=\sum_l \pm Q_k^{(l)} \tag{32}$$

where $\bar{\Omega}_k^{(n)}$ (Eq. (9a)) can be re-written as

$$\bar{\Omega}_k^{(n)}=\Omega_k^{(j)}-\Omega_k^{(i)}+h_n U_k^{(n)} \tag{33}$$

in which $h_n\left(=y_n^{(j)}-y_n^{(i)}\right)$ represents the length of the *n*-th link element as shown in Fig. 2(b). For link elements included in open sections and branches, Eq. (32) can be simplified to

$$\bar{\Omega}_k^{(n)}=0 \tag{34}$$

The remaining unknown warping displacement represents a uniform extension and is conveniently chosen so that the *k*-th warping distribution is orthogonal to the extension. This can be achieved by requiring that the *k*-th warping mode has nil average

$$\int_C \Omega_k(s)ds=0 \tag{35}$$

3.2 Warping eigenvalue problem (WEP)

The warping eigenvalue problem is performed to a frame representing the cross-section able to deform only in the out-of-plane direction. In this case, the eigenproblem is denoted as WEP and the sought GBT (shear) modes are defined by the dynamic modes of the frame. The dynamic analysis is carried out by means of the finite element method (Fig. 3) by considering the following three finite element representations: (i) FE_1 (Fig. 4(a)) represents a 2 DOF finite element with linear (Lagrangian) polynomial shape functions, (ii) FE_2 (Fig. 4(b)) depicts a 3 DOF finite element with parabolic (Lagrangian) shape functions, and (iii) FE_3 (Fig. 4(c)) denotes a 5 DOF finite element with quartic (Lagrangian) polynomial interpolating functions.

The algebraic eigenvalue problem related to the entire cross-section can then be written as

$$\left(\mathbf{K}_W-\lambda\mathbf{M}_W\right)\boldsymbol{q}_W=\mathbf{0} \tag{36}$$

where $\mathbf{K}_W$ is the section stiffness matrix, $\mathbf{M}_W$ represents its mass matrix, $\boldsymbol{q}_W$ is the out-of-plane displacement vector and λ is the squared natural frequency of vibration.

The partial interaction response exhibited in the longitudinal direction for the shear connection is included by means of a 2 DOF spring element (Fig. 4(a)) with negligible mass. This element is used to connect the different components forming the cross-section and its degrees of freedom include the out-of-plane displacements at the shear connection interface. For the *n*-th link element, the stiffness matrix can be written as

$$K_W^{(n)}=k_L^{(n)}\begin{bmatrix}1 & -1\\ -1 & 1\end{bmatrix} \tag{37}$$

where $k_L^{(n)}$ is the longitudinal shear connection rigidity of the *n*-th shear connector. The eigenvectors obtained from Eq. (36) define the nodal displacements of the *J* shear modes.

4. Application

The proposed GBT formulation is validated in this section by considering a composite steel-concrete beam subjected to an eccentric load. For this purpose, a composite member reported in reference (Hanaor 2000) is used as a case study. Its length is equal to 5m and its concrete slab has a thickness of 50 mm. The steel components consist of two Z cold formed steel profiles and a bottom flat steel plate, as shown in Fig. 5. All steel elements have thickness of 2 mm. The elastic modulus of the steel is 200 GPa and the one for the concrete is 35 GPa. Poisson's ratio of 0.3 and 0.2 are specified for the steel and concrete, respectively. The member is taken as simply-supported and is free to warp at the end supports, while it is restrained from warping at mid-span. A uniform pressure of 5 kPa is applied to the concrete slab as shown in Fig. 5(a). Three levels of shear connection rigidities have been considered and expressed in terms of dimensionless parameters $\alpha_L L$ and $\alpha_T L$ (referred to the longitudinal and transverse shear connection, respectively), commonly used for two-layered composite beams, e.g., (Taig and Ranzi 2015, 2016). In particular, $\alpha_L L=\alpha_T L=1$ depict a weak shear connection stiffness, while $\alpha_L L=\alpha_T L=5$ and $\alpha_L L=\alpha_T L=20$ denote a medium and a stiff shear connection rigidity, respectively.

The conventional, extensional and shear modes for the cross-section of Fig. 5(a) are obtained with the proposed procedure. Representative subsets of these modes have been presented for illustrative purposes in Figs. 6-8 by considering the first 6 modes of each set of modes. The plotted modes have been obtained with a medium shear connection rigidity (i.e., $\alpha_L L=\alpha_T L=5$) using FE_3 finite elements for both PEP and WEP.

The conventional modes are outlined in Fig. 6. The first three modes consist of the in-plane rigid modes followed by the mixed in-plane translational-flexural modes. These modes do not exhibit axial elongations of the elements composing the cross-section. The partial interaction is described in these modes by the presence of transverse and longitudinal slips represented by deformations modes $\bar{V}_k^{(n)}, \bar{\Omega}_k^{(n)}$ introduced in Eqs. (8) and (9(a)), respectively.

Fig. 7 presents the representative extensional modes that are represented in terms of both in-plane displacements (*uv*) and tangential displacements *u*. Due to the presence of the closed loops, these modes are described not only by extension and/or shortening of the elements forming the cross-sections but are coupled with flexural deformations, as well depicted, for example, for modes *E*1, *E*3 and *E*4.

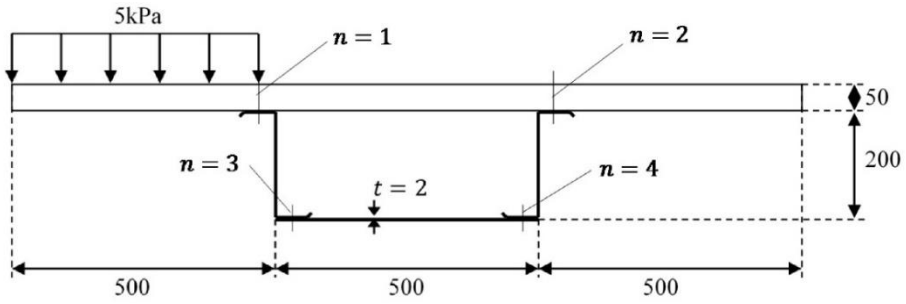

(a) built-up cross-section

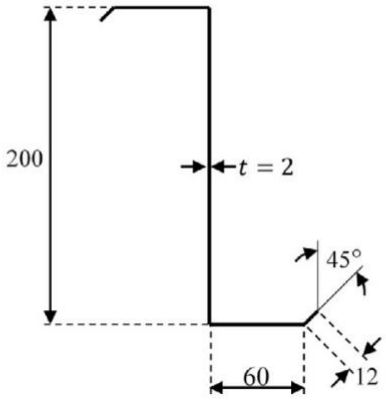

(b) geometry of the Z-section

Fig. 5 Partially-closed composite steel-concrete member (Hanaor 2000). All dimension are in mm

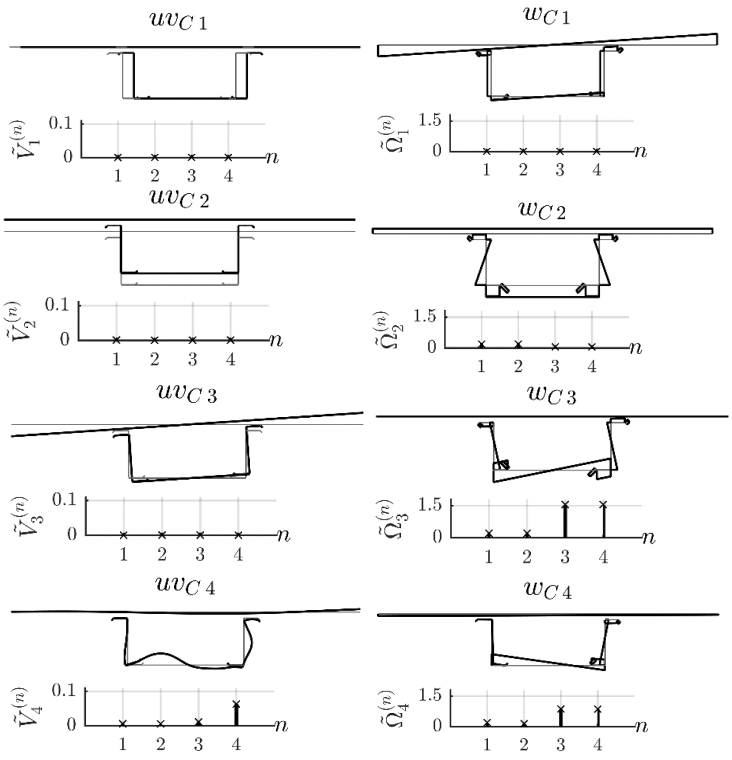

Continued-

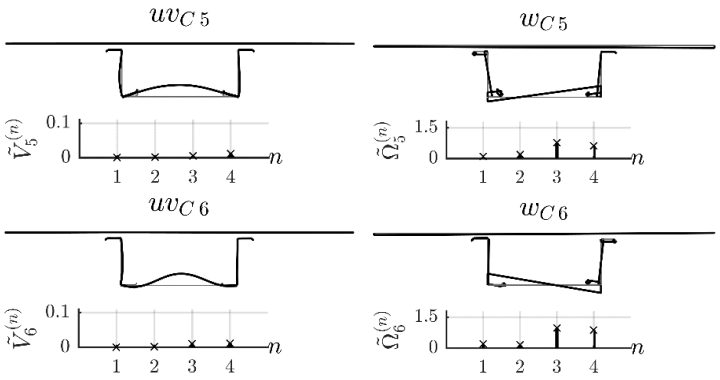

Fig. 6 Partially-closed composite steel-concrete member: conventional modes

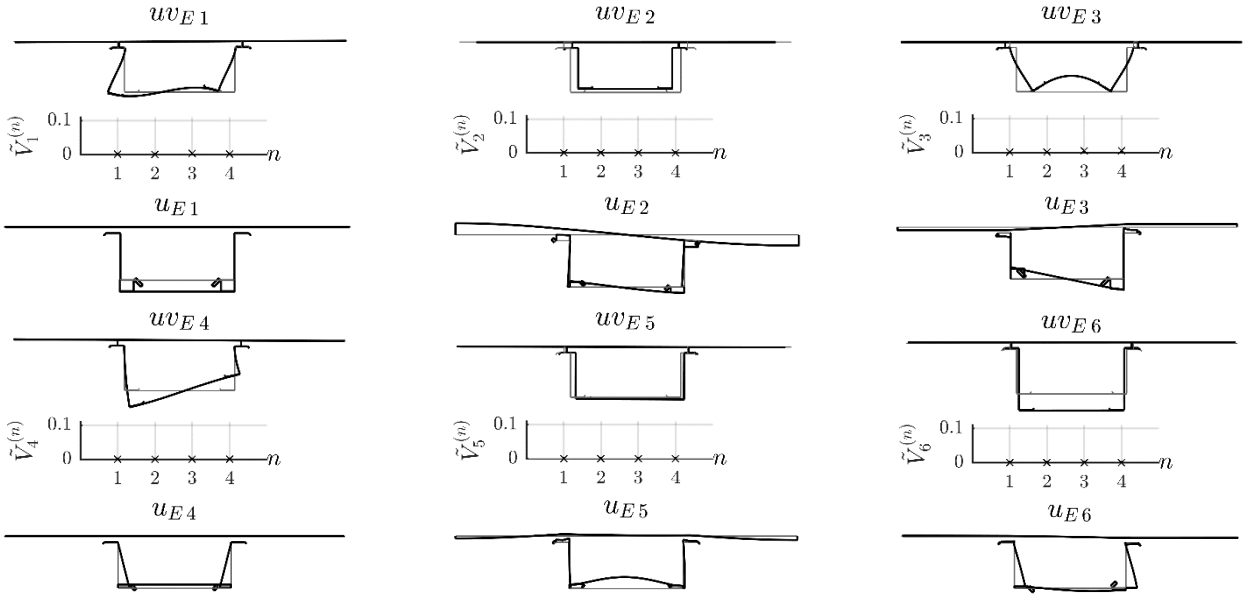

Fig. 7 Partially-closed composite steel-concrete member: extensional modes

The extensional modes do exhibit deformations associated with the partial interaction. The representative shear modes are illustrated in Fig. 8. In particular mode *S*1 represents the case of uniform extension, while the other shear modes describe warping fields that might include partial interaction effects as defined by $\overline{W}_k^{(n)}$ of Eq. (9(b)).

In these figures, the normalised longitudinal and transverse slips are presented for each mode and are expressed dividing the absolute slip value by the maximum value of either the warping (for the longitudinal slip) or the in–plane displacement (for the transverse slip) as follows

$$\tilde{V}_k^{(n)} = \frac{\left|\overline{V}_k^{(n)}\right|}{\max\left(\left|U_k\right|,\left|V_k\right|\right)};\tilde{\Omega}_k^{(n)} = \frac{\left|\overline{\Omega}_k^{(n)}\right|}{\max\left(\left|\Omega_k\right|\right)};\tilde{W}_j^{(n)} = \frac{\left|\overline{W}_j^{(n)}\right|}{\max\left(\left|W_j\right|\right)} \quad (38a,b,c)$$

A shell element model developed in ABAQUS/Standard (Dassault Systèmes Simulia 2008) is been used to validate the results calculated with the proposed GBT procedure. Representative comparisons are plotted in Fig. 9 considering the case of $\alpha_L L = \alpha_T L = 1$ in the implementation and solution of the PEP and WEP. All variables have been plotted at the member coordinate in which they reach their maximum values. This occurs at mid-span (i.e., $z = L/2$) for the in-plane displacements (*uv*), tangential and normal membrane and flexural stresses (i.e., $\sigma_s^{(M)}, \sigma_z^{(M)}, \sigma_s^{(F)}, \sigma_z^{(F)}$), while warping displacements *w* and shear stress components (i.e., $\tau_{sz}^{(M)}, \tau_{sz}^{(F)}$) reach their maximum at the end sections (i.e., $z = 0, L$). For clarity, the plotted variables have been suitably scaled and the maximum (absolute) value of each stress component has been specified.

The results determined using different levels of shear connection rigidities have been used in Fig. 10. When considering weak shear connection (i.e., $\alpha_L L = \alpha_T L = 1$), there is a negligible interaction taking place between the components forming the cross-section. This is shown, for example, by the two stiffer Z sections taking most of the load, as highlighted by the distributions of the membrane stresses $\sigma_z^{(M)}$ and membrane shear stresses $\tau_{sz}^{(M)}$.

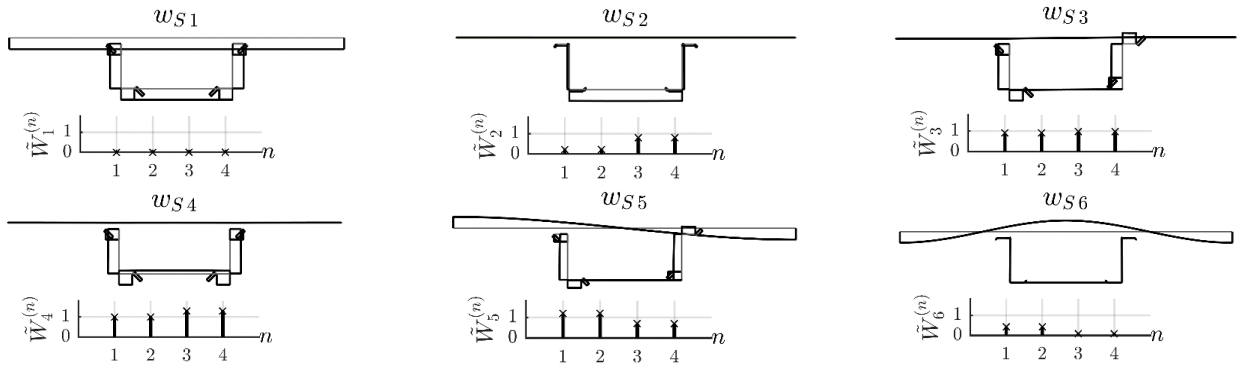

Fig. 8 Partially-closed composite steel-concrete member: shear modes

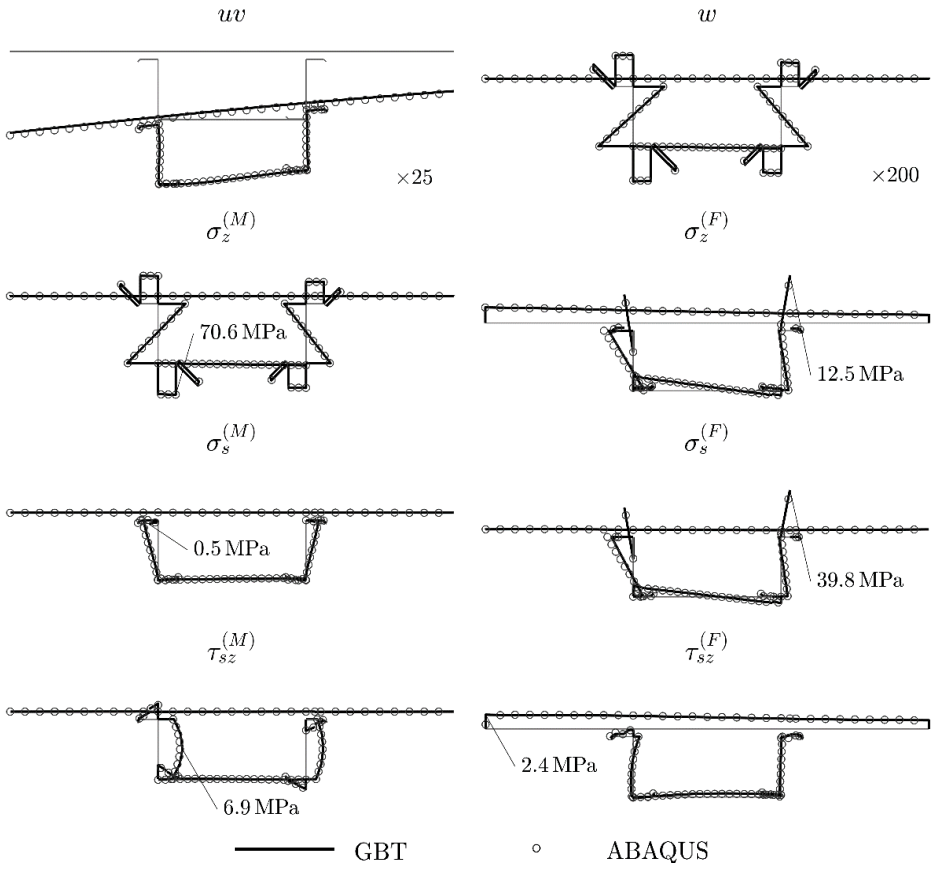

Fig. 9 Partially-closed composite steel-concrete member: displacements and stress fields with weak shear connection ($\alpha_L L = \alpha_T L = 1$)

For medium shear connection rigidities (i.e., $\alpha_L L = \alpha_T L = 5$), the four components start to act compositely, and the multi-component member behave as a partially closed cross-section. In this case, the stress distributions, e.g., membrane stress $\sigma_z^{(M)}$ and the membrane shear stress $\tau_{sz}^{(M)}$, are resisted over the entire cross-section, therefore depicting how the different components are working together. The case of $\alpha_L L = \alpha_T L = 20$ shows a stiffer response as expected and a higher interaction between the components forming the cross-section. In all cases, the GBT results well match the values calculated with the ABAQUS model.

Comparisons between the values calculated using different finite elements (i.e., FE_1, FE_2 and FE_3 in Fig. 4) in the GBT cross-section analysis are presented in Fig. 11 and are presented considering the results obtained with the FE_3 finite element (Fig. 4(c)) for reference in the following. The variations in displacements are negligible as the calculated in-plane and out-of-plane displacements (i.e., *u*, *v* and *w*) produce maximum errors within 0.05% for both the FE_1 (Fig. 4(a)) and FE_2 (Fig. 4(b)), respectively.

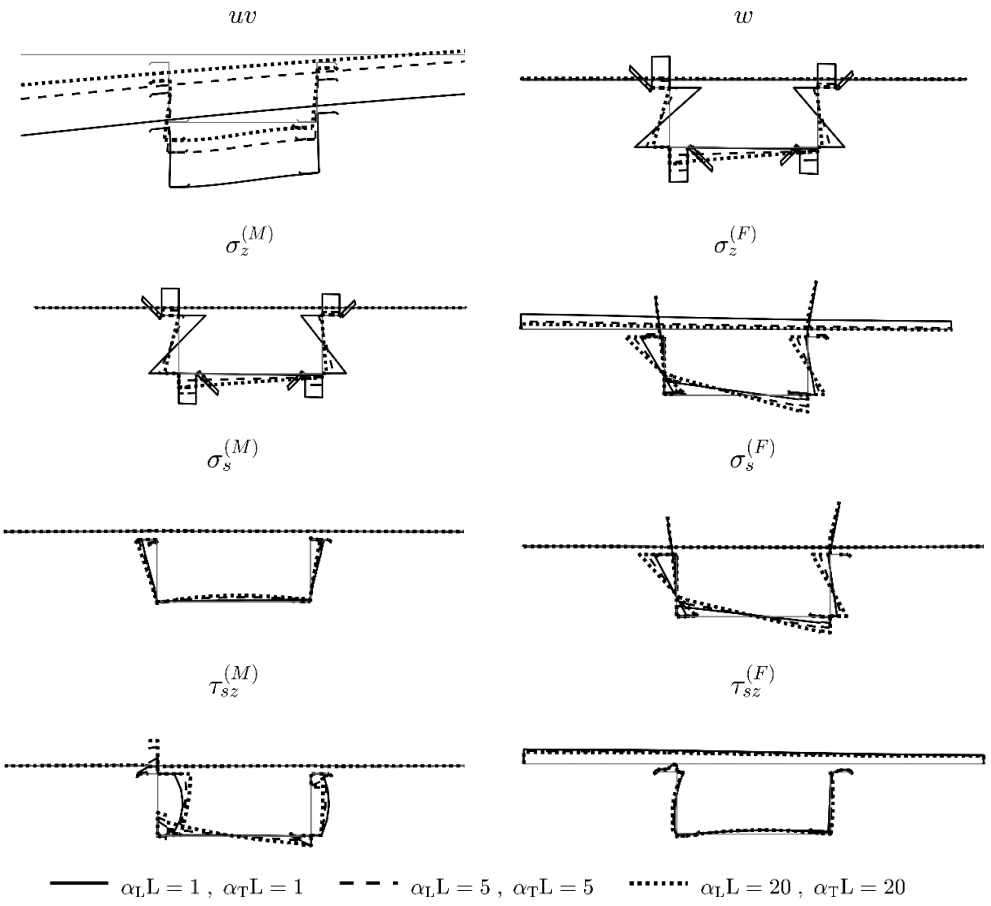

Fig. 10 Partially-closed composite steel-concrete member: displacements and stress fields for different levels of shear connection stiffness

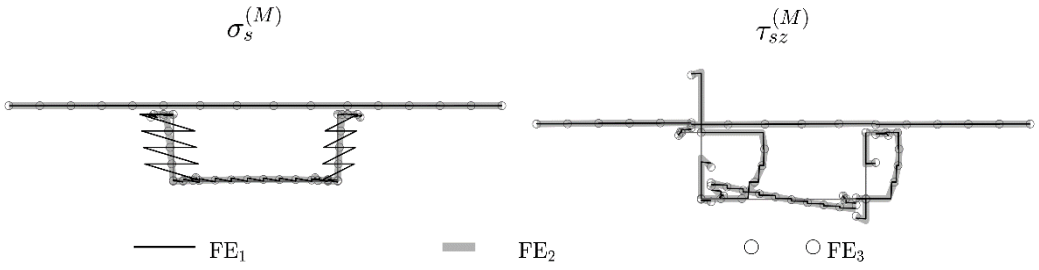

Fig. 11 Partially-closed composite steel-concrete member: comparison of stress fields $\sigma_s^{(M)}$ and $\tau_{sz}^{(M)}$ for different types of finite elements

Similar considerations can be made for the flexural stresses, i.e., $\sigma_s^{(F)}, \sigma_z^{(F)}, \tau_{sz}^{(F)}$ and membrane longitudinal stress, i.e., $\sigma_z^{(F)}$, with maximum errors calculated using FE_1 and FE_2 within 1.5% and 0.01%, respectively. Different results are obtained when considering the membrane transverse stress $\sigma_s^{(M)}$ (that depends on $U_{k,s}$, Ω_k and W_j as outlined in Eq. (5)) and the shear stress $\tau_{sz}^{(M)}$ (that depends on U_k, $\Omega_{k,s}$ and $W_{j,s}$ as shown in Eq. (5)). These results are influenced by the orders of polynomials adopted in the cross-section analysis. In particular, when using the FE_1 finite elements, discontinuities are observed between adjacent finite elements as illustrated in Fig. 11.

These are produced by the fact that the cross-section modes U_k, Ω_k and W_j contribute with different order polynomials to the evaluations of $\sigma_s^{(M)}$ and $\tau_{sz}^{(M)}$, and therefore lead to a locking problem. This aspect can be avoided by modifying the order of the finite element polynomials adopted in the GBT cross-section analysis to ensure a consistent set of generalised displacements. This

can be achieved, for example, by adopting parabolic shape functions (as carried out for element FE_2 – Fig. 4(b)) instead of linear ones (for element FE_1 – Fig. 4(a)) in the finite elements used for the determination of U_k, Ω_k and W_j. In doing so, the results calculated with the FE_2 finite elements match those obtained with the reference solution, with maximum differences within 0.5%.

5. Conclusions

This paper presented a new approach for the first-order (linear elastic) multi-component partial interaction analysis. The particularity of this procedure is to identify a suitable set of deformation modes capable of describing both longitudinal and transverse partial interactions taking place at the interface plane between the adjacent components while accounting for the cross-sectional deformability. The deformation modes are described by the eigenmodes determined by solving a planar and a warping eigenvalue problem of a planar frame that represents the cross-section. The partial interaction has been introduced in the GBT cross-section step by specifying deformable spring finite elements at the shear connection location. The proposed approach has been validated against the numerical values obtained by means of a shell finite element model developed in ABAQUS/Standard by considering a case study of a multi-component member subjected to an eccentric load. For illustrative purposes, representative results have been presented to highlight the ease of use of the proposed methodology and to show how the structural response is influenced by different rigidities of the interface shear connection. The importance of selecting a consistent set of polynomials for the finite element representation specified for the GBT cross-section analysis has also been discussed. Locking problems have been shown to occur when this consistency is not satisfied.

Acknowledgements

The work in this article was supported by the Australian Research Council through its Future Fellowship scheme (FT140100130) and by Material & Structures Research Cluster of the University of Sydney.

References

Ádány, S. and Shafer, B.W. (2006), "Buckling mode decomposition of single-branched open cross-section members via finite strip method: Application and examples", *Thin Wall. Struct.*, **44**, 585-600.

Ádány, S. and Shafer, B.W. (2008), "A full modal decomposition of thin-walled, single branched open cross-section members via the constrained finite strip method", *J. Constr. Steel Res.*, **64**, 12-29.

Adekola, A.O. (1968), "Partial interaction between elastically connected elements of a composite beam", *Int. J. Solids Struct.*, **4**, 1125-1135.

Al-Deen, S., Ranzi, G. and Uy, B. (2015), "Non-uniform shrinkage in simply-supported composite steel-concrete slabs", *Steel Compos. Struct.*, **18**(2), 375-394.

Bathe, K.J. (2006), *Finite Element Procedure*, Prentice Hall, New Jersey.

Casafront, M. and Marimon, M.M. (2009), "Calculation of pure distorsional elastic buckling loads of members subjected to compression via finite element method", *Thin Wall. Struct.*, **47**, 701-729.

Chakrabarti, A., Sheikh, A.H., Grifith, M. and Oehlers, D.J. (2012), Analysis of composite beams with partial shear interaction using a higher order beam theory", *Eng. Struct.*, **36**, 283-291.

Dassault Systèmes Simulia, (2008), *ABAQUS User's Manual", version 6.8EF-2*, Dassault Systèmes Simulia Corp., Providence, RI, USA.

Dezi, L., Gara, F. and Leoni, G. (2003), "Shear-lag effect in twin-girder composite decks", *Steel Compos. Struct.*, **3**(2), 111-122.

Dezi, L., Gara, F. and Leoni, G. (2006), "Effective slab width in prestressed twin-girder composite decks", *J. Struct. Eng.*, **132**(9), 1358-1370.

Eccher, G., Rasmussen, K.J.R. and Zandonini, R. (2008), "Linear elastic isoparametric spline finite strip analysis of perforated thin-walled structures", *Thin Wall. Struct.*, **46**, 242-260.

Gara, F., Carbonari, S., Leoni, G. and Dezi, L. (2014), "A higher order steel-concrete composite beam model", *Eng. Struct.*, **80**, 260-273.

Gonçalves, R. and Camotim, D. (2010), "Steel-concrete composite bridge analysis using Generalised Beam Theory", *Steel Compos. Struct.*, **10**, 223-243.

Hanaor, A. (2000), "Tests of composite beams with cold-formed sections", *J. Constr. Steel Res.*, **54**, 245-264.

Henriques, D., Gonçalves, R. and Camotim, D. (2015) "A physically non-linear GBT-based finite element for steel and steel-concrete beams including shear lag effects", *Thin Wall. Struct.*, **90**, 202-215.

Henriques, D., Gonçalves, R. and Camotim, D. (2016) "GBT-based finite element to assess the buckling behaviour of steel-concrete composite beams", *Thin Wall. Struct.*, **107**, 207-220.

Li, D., Uy, B., Patel, V. and Aslani, F. (2016), "Behaviour and design of demountable steel column-column connections", *Steel Compos. Struct.*, **22**(2), 429-448.

Liu, X., Bradford, M.A., Chen, Q.J. and Ban, H. (2016), "Finite element modelling of steel-concrete composite beams with high-strength friction-grip bolt shear connectors", *Finite Elem. Anal. Des.*, **108**, 54-65.

Luongo, A. (2001), "Mode localization in dynamics and buckling of linear imperfect continuous structures", *Nonlinear Dyn.*, **25**, 133-156.

Newmark, N.M., Siess, C.P. and Viest, I.M. (1951), "Test and analysis of composite beams with incomplete interaction", *Proc. Soc. Exp. Stress Anal.*, **9**(1), 75-92.

Nguyen., Q.H., Hjiai, M. and Lai, V.A. (2014), "Force-based FE for large displacement inelastic analysis of two-layer Timoshenko beams with interlayer slips", *Finite Elem. Anal. Des.*, **85**, 1-10.

Piccardo, G., Ranzi, G. and Luongo, A. (2014), A complete dynamic approach to the Generalized Beam Theory cross-section analysis including extension and shear modes", *Math Mech Solids*, **19**, 900-924.

Ranzi, G. and Gilbert, R.I. (2015), *Structural Analysis: Principles, Methods and Modelling*, Spoon Press,

Ranzi, G. and Luongo, A. (2011), "A new approach for thin-walled member analysis in the framework of GBT", *Thin Wall. Struct.*, **49**, 1404-1414.

Schardt, R. (1989), *Verallgemeinerte Technicsche Biegetheory*, Springler-Verlag, Berlin, Germany.

Silva, N.F., Silvestre, N. and Camotim, D. (2006), "GBT formulation to analyse the buckling behaviour of frp composite

branched thin-walled beams", *Proceedings of the III European Conference on Computational Mechanics Solids, Structures and Coupled Problems in Engineering, Lisbon, Portugal, June*.

Silvestre, N. and Camotim, D. (2002), "First-order generalised beam theory for arbitrary orthotropic materials", *Thin Wall. Struct.*, **40**, 755-789.

Su, Q., Yang, G. and Bradford, M.A. (2014), "Static behaviour of multi-row stud shear connectors in high-strength concrete", *Steel Compos. Struct.*, **17**(6), 967-980.

Taig, G. and Ranzi, G. (2015), "Generalised beam theory (GBT) for composite beams with partial shear interaction", *Eng. Struct.*, **99**, 582-602.

Taig, G. and Ranzi, G. (2016), "Generalised beam theory for composite beams with longitudinal and transverse partial interaction", *Math. Mech Solids*, DOI: 10.1177/1081286516653799.

Taig, G., Ranzi, G. and D'Annibale, F. (2015b) "An unconstrained dynamic approach for the Generalised Beam Theory", *Contin. Mech. Thermodyn*, **27**, 879-904.

Taig, G., Ranzi, G., Dias-da-Costa, D., Piccardo, G and Luongo, A. (2015a), "A GBT model for the analysis of composite steel-concrete beams with partial shear interaction", *Structures*, **4**, 25-37.

Vlasov, V.Z. (1961), *Thin-Walled Elastic Beams*, Monson, Jerusalem, Israel.

Vrcelj, Z. and Bradford, M.A. (2008), "A simple method for the inclusion of external and internal supports in the spline finite strip method (SFSM) of buckling analysis", *Comput. Struct.*, **86**, 529-544.

DL

Appendix

$$\mathbf{B}=\begin{bmatrix} \mathbf{B}^{11} & \mathbf{0}_{K\times K} & \mathbf{B}^{13} & \mathbf{0}_{K\times J} & \mathbf{B}^{15} \\ & \mathbf{B}^{22} & \mathbf{0}_{K\times K} & \mathbf{B}^{24} & \mathbf{0}_{K\times J} \\ & & \mathbf{B}^{33} & \mathbf{0}_{K\times J} & \mathbf{B}^{35} \\ & \text{sym} & & \mathbf{B}^{44} & \mathbf{0}_{J\times J} \\ & & & \mathbf{0}_{J\times J} & \mathbf{B}^{55} \end{bmatrix} \quad \text{(A1)}$$

$$B_{hk}^{11}=\sum_{\alpha=1}^{N_m}\int_{A_\alpha}\frac{E_\alpha}{1-\nu_\alpha^2}\left(U_{h,s}U_{k,s}+y^2V_{h,ss}V_{k,ss}\right)dA+\sum_{n=1}^{N_{sc}}k_T^{(n)}\bar{V}_h^{(n)}\bar{V}_k^{(n)} \quad \text{(A2)}$$

$$B_{hk}^{13}=\sum_{\alpha=1}^{N_m}\int_{A_\alpha}\frac{\nu_\alpha E_\alpha}{1-\nu_\alpha^2}\left(U_{h,s}\Omega_k+y^2V_{h,ss}V_k\right)dA; \qquad B_{hj}^{15}=\sum_{\alpha=1}^{N_m}\int_{A_\alpha}\frac{\nu_\alpha E_\alpha}{1-\nu_\alpha^2}U_{h,s}W_j dA \quad \text{(A3,4)}$$

$$B_{hk}^{22}=\sum_{\alpha=1}^{N_m}\int_{A_\alpha}G_\alpha\left[\left(\Omega_{h,s}+U_h\right)\left(\Omega_{k,s}+U_k\right)+4y^2V_{h,s}V_{k,s}\right]dA+\sum_{n=1}^{N_{sc}}k_L^{(n)}\bar{\Omega}_h^{(n)}\bar{\Omega}_k^{(n)} \quad \text{(A5)}$$

$$B_{hj}^{24}=\sum_{\alpha=1}^{N_m}\int_{A_\alpha}G_\alpha\left(\Omega_{h,s}+U_h\right)W_{j,s}dA+\sum_{n=1}^{N_{sc}}k_L^{(n)}\bar{\Omega}_h^{(n)}\bar{W}_j^{(n)} \quad \text{(A6)}$$

$$B_{hk}^{33}=\sum_{\alpha=1}^{N_m}\int_{A_\alpha}\frac{E_\alpha}{1-\nu_\alpha^2}\left(\Omega_h\Omega_k+y^2V_hV_k\right)dA; \qquad B_{hj}^{35}=\sum_{\alpha=1}^{N_m}\int_{A_\alpha}\frac{E_\alpha}{1-\nu_\alpha^2}\Omega_h W_j dA \quad \text{(A7,8)}$$

$$B_{ij}^{44}=\sum_{\alpha=1}^{N_m}\int_{A_\alpha}G_\alpha W_{i,s}W_{j,s}dA+\sum_{n=1}^{N_{sc}}k_L^{(n)}\bar{W}_i^{(n)}\bar{W}_j^{(n)}; \qquad B_{ij}^{55}=\sum_{\alpha=1}^{N_m}\int_{A_\alpha}\frac{E_\alpha}{1-\nu_\alpha^2}W_iW_j dA \quad \text{(A9,10)}$$

$$C_{hk}=\sum_{\alpha=1}^{N_m}\int_{A_\alpha}\frac{E_\alpha}{1-\nu_\alpha^2}U_{h,s}U_{k,s}dA \quad \text{(A11)}$$

$$D_{hk}=\sum_{\alpha=1}^{N_m}\int_{A_\alpha}\frac{E_\alpha}{1-\nu_\alpha^2}y^2V_{h,ss}V_{k,ss}dA+\sum_{n=1}^{N_{sc}}k_T^{(n)}\bar{V}_h^{(n)}\bar{V}_k^{(n)} \quad \text{(A12)}$$

$$\boldsymbol{q}=\begin{bmatrix}\boldsymbol{q}^{(1)} & \boldsymbol{q}^{(2)} & \boldsymbol{q}^{(3)}\end{bmatrix}^T \quad \text{(A13)}$$

$$q_h^{(1)}=\int_C\left[p_s(s,z)U_h(s)+p_y(s,z)V_h(s)\right]ds \quad \text{(A14)}$$

$$q_h^{(2)}=\int_C p_z(s,z)\Omega_h(s)ds; \qquad q_j^{(3)}=\int_C p_z(s,z)W_j(s)ds \quad \text{(A15,16)}$$

$$\boldsymbol{A}=\begin{bmatrix}\mathbf{I}_K & \mathbf{0}_{K\times J}\\ \mathbf{I}_K\partial & \mathbf{0}_{K\times J}\\ \mathbf{I}_K\partial^2 & \mathbf{0}_{K\times J}\\ \mathbf{0}_{J\times K} & \mathbf{I}_J\\ \mathbf{0}_{J\times K} & \mathbf{I}_J\partial\end{bmatrix}; \qquad \boldsymbol{B}=\begin{bmatrix}\mathbf{I}_K & \mathbf{0}_{K\times J}\\ \mathbf{I}_K\partial & \mathbf{0}_{K\times J}\\ \mathbf{0}_{J\times K} & \mathbf{I}_J\end{bmatrix} \quad \text{(A17,18)}$$

where $\mathbf{0}_{N\times M}$ is zero matrix of size ($N\times M$); sub-matrices $\mathbf{B}^{11}$, $\mathbf{B}^{13}$, $\mathbf{B}^{22}$, $\mathbf{B}^{33}$ have size ($K\times K$); sub-matrices $\mathbf{B}^{13}$, $\mathbf{B}^{24}$, $\mathbf{B}^{35}$ possess size ($K\times J$); sub-matrices $\mathbf{B}^{44}$, $\mathbf{B}^{55}$ have size ($J\times J$); sub-vectors $\boldsymbol{q}^{(1)}$ and $\boldsymbol{q}^{(2)}$ have dimensions of ($K\times 1$); sub-vector $\boldsymbol{q}^{(3)}$ has size ($J\times 1$); $\mathbf{I}_N$ is the identity matrix of size ($N\times N$); ∂ denotes differentiation with respect to z; N_m depicts the number of materials forming the cross-section; A_α is the area of the *α-th* material.